Abstract

This study examines heat transfer and mass diffusion in a unique fluid motion close to a rapidly stretching boundary. Across this flow, a magnetic field acts sideways, tying changes in velocity, temperature, and concentration into one linked system. Rather than remain as tangled equations in time and space, these relationships simplify using symmetry-driven transformations. The solution domain, originally stretching from zero to infinity, shifts to a set interval - zero to one - by rescaling the variable dimensions. Steady answers come through even as accuracy climbs, thanks to wavy math tools. Not one image but several tracks how numbers without units affect pace, temperature, flow - line by line. From each graph, a sharper sense grows about clashes between magnetic fields, heat, and mixed-in materials. Hidden threads emerge in goopy fluids pulled harder, stretching quicker every moment. Most noticeable? The way push, movement, and resistance lock together tighter when strain increases.

What shows up comes from seeing things placed next to one another, not from trying to figure it out blindly. A picture builds when pieces sit close, letting shapes speak without guessing. Close placement lets eyes catch what minds might miss. Seeing repeats happens because items align, making differences and similarities visible. Without lining them up, patterns stay hidden. Side-by-side makes the invisible seen

Keywords: Casson fluid flow, MHD, exponentially stretching sheet, Taylor wavelet.

Nomenclature

B	Variable magnetic field (T)	T_m	Mean fluid temperature
B_0	Magnetic field strength	T_0	Parameter of the temperature allocation
C	Concentration($mol\ m/^3$)	u_0	Velocity parameter of the stretching surface($m\ s/$)
C_0	Parameter of the concentration allocation in the stretching surface	$u\ v$,	Velocities in $x-$and $y-$ directions ($m\ s/$)
C_P	Specific heat capacity ($J\ kg\ C/^0$)	$x\ y$,	Cartesian coordinates(m)
C_S	Concentration susceptibility		
D_f	Dufour number	**Greek Symbols**	
g^*	Acceleration due to gravity	□	Thermal diffusivity
Gr	Thermal Grashof number	□	Cassonfactor
K_T	Thermal diffusion ratio(m^2/s)	□$_C$	Coefficient of solutal extensions
L	Plate's characteristic length	□$_T$	Coefficient of thermal extension
M	Magnetic number (Hartmann number)	□	Dynamic viscosity
N	Buoyancy ratio	□	Non-dimensional concentration
Pr	Prandtl number	□	Fluid density ($kg\ m/^3$)
Re	Reynolds number	□	Electrical conductivity($S\ m/$)
Ri	Mixed convection parameter	□	Non-dimensional temperature

S	Squeeze number	$\square$	Kinematic viscosity$\left(m^2 / s\right)$
Sc	Schmidt number	$\square$	Stream function
Sr	Soret number	$\square$	Location $\left(x\ L/\right)$
T	Temperature (K)		

1. Introduction

Floating currents behave strangely - magnetohydrodynamics studies their dance. Not counting every speck, researchers pretend charges are a single flowing goop. From that trick, large behaviors rise: shoves, drags, stillness, tremors. Imagine solar tantrums or human-made fire-fogs twisting inside hidden pressures. One aim stands out: see how light force and magnetic hands pull on heavy streams creeping through porous traps. Out of thin air, a magnetic shove crosses paths with moving metal, waking up electric energy within. This sudden charge pushes against the flow - twisting how fast things move, which way they turn, sometimes even changing how much gets blocked.
Magnetic fields change how liquids move, seen in tasks like guiding superheated gas, forming metal parts, cooling reactors, or steering plastic flow in factories. Instead of starting with basics, Abbas and colleagues checked what happens when Casson–Sutterby-like fluids slide over a curving stretchy shape that speeds up. Mabood's study took another path - using homotopy tricks to probe fluid shifts above a fast-expanding sheet giving off rays. Ahmad's crew focused elsewhere: run-of-the-mill thick liquids crawling on swiftly widening surfaces buried in porous stuff. Midway through their work, Mahabaleshwar's team examined how tilt-driven MHD flows mix heat and matter when the Richardson factor steps in. Away from the usual route, work by Patil and Kumbarwadi [5] looked at magnetohydrodynamics where heat gradients and diffusion mix above rapidly stretching sheets. Machines often use liquids ignoring Newton's rule for thickness - these shift oddly when moving or transferring warmth. The Casson framework [6–8] helps explain them, showing how they resist flow until pushed, then become runnier under stress. Think of goopy soups full of bits [9], stuff similar to blood [10], even printer ink - they line up close enough. Since real-life uses pop up everywhere, watching how Casson flows react to magnets along with shifts in temperature and material still matters deeply in fluid science.

Out past the edge, things get tricky as sheets pull apart quicker over time. Fluids act different nearby, their rhythm tied to how fast the surface stretches below them. Think of plastic films rolling out endlessly, or delicate fibers drawn thin under pressure. Speed climbs oddly here - faster not by steps but leaps toward the outer parts. Production lines bump into this often, moving material while tension builds along its path. Math becomes a key tool, peeling back layers in motion puzzles through structured models. At play is Navier–Stokes, shaped tightly by fixed start and boundary rules. Figuring out these numbers shows how speed, temperature, and heat flow connect. Results like these guide adjustments in actual equipment. In one case, Animasaun's group studied a dense fluid - the sort that barely flows when pressure is weak - applying homotopy analysis to surfaces stretching fast. They accounted for matter pulling through the surface, also internal warmth building up in the liquid. When radiation plays a role, bending shapes shift how thermal energy travels in magnetized liquids,

according to Anantha Kumar and colleagues. Close to speeding sheets, tiny particles change how heat moves - findings uncovered by Mustafa's team reveal. Not just in slim pockets of air, fluids with springy traits behave unusually when surfaces shoot outward - Khan took a deep look there.
Warmth and dissolved substances traveling hand in hand inside fluids - this pairing goes by double diffusion - emerge whenever temperature contrasts meet uneven compositions. These dual imbalances guide how stuff and heat disperse within flowing matter. From shifting rock layers underfoot to cells doing their jobs, chemical reactors humming quietly, and systems producing electricity, such behavior turns up often. Examining microscopic swirls reacting near porous zones where motion varies point to point, research led by Shamshuddin dug into what occurs during those interactions. At another turn, work guided by Mouli applied sharp mathematical methods to follow hot-cold blending plus solute wandering across surfaces that stretch while soaked in fluid that resists flow more than water does. Meanwhile, Hayat's team studied how magnetism influences heating and mixing in moving fluids. In a different direction, Srinivasen examined high-pressure liquid mixtures alongside microscopic vibrations.

Wavelet theory lately grabs attention, handling tricky math problems tied to liquid motion and how things travel through it. Older ways - think finite pieces, grid steps, or frequency methods - often miss small shifts seen at varied levels; wavelets catch them more easily. Some kinds - Chebyshev [19], Haar [20], Legendre [21], Laguerre [22], basic B-splines [23], Hermite [24,25], even Bernoulli forms [26–30] - solve actual cases where heat spreads or liquids move. Work moves forward steadily here, proving these tools now matter deeply when simulating fluids in motion.

Out of nowhere, fluid reactions to magnets and warmth get a new look. Through wavy patterns guided by Taylor's methods, stubborn math behind heavy flows on rapidly expanding surfaces begins to untangle. One stage follows another - not simply connected - revealing how temperature and salt movement dance when magnetic force tugs at the stream. The thick stuff gains character, thanks to Casson's influence, turning classroom theories into something resembling actual production floors. Out of changing figures come shapes - quick, warm, mixed - edges blur where layers meet. Strong machines chew through messy physics, inching ahead while old ways fade behind.

2. Problem assumptions and mathematical formulation

A smooth, flat surface moves steadily upward, pulling the thick liquid next to it into motion. Because of this pull, how fast the fluid moves, its warmth, and makeup shift close to the boundary - see sketch one. We set up our measuring lines so that forward movement follows the horizontal line, while distance from the wall goes straight out sideways. Far off from the wall, the liquid barely stirs, holding steady heat and mix levels. This setup captures slow, layered sliding without sudden changes. Here, we include how Dufour and Soret effects shape the results. Energy moves when differences in mix happen - that is the Dufour part. On the flip, material spreads if warmth shifts around - this shows up as Soret influence. Together, these links tie heat and mixture together, changing how both move near surfaces. We build rules for mass, motion, heat, and substance spread using slim-layer and floating-fluid ideas. Such choices drop most density changes, yet keep them alive inside lift forces, making it easier to see how heat and blend shifts steer movement patterns.
Figuring out how the liquid moves means using the Casson fluid idea [6]. Not just limited to smooth flow patterns, this approach fits stuff that won't budge until enough force hits it. Once pushed hard

enough, what seemed solid starts acting runny. Think of things such as blood, blended foods, thick factory mixtures - same pattern shows up there too. Its math rule goes like this, if you look at reference

$$\sqrt{\xi} = \sqrt{\xi} + \mu \sqrt{\frac{du}{dy}_{xy}} \quad {}_0 \quad \sqrt{}_0 \quad \text{for} \quad \xi_{xy} > \xi_0$$

$$\frac{du}{dy} \geq 0, \qquad \text{for} \xi_{xy} < \xi_0$$

where ξ_{xy} is the shear stress, ξ_0 is the yield stress, μ_0 is a viscosity, and $\frac{du}{dy} \geq 0$ is the shear rate.

Adding magnetic forces along with thermal and solute diffusion plus non-Newtonian fluid behavior gives a full picture of how motion, warmth, and material spread interact. With such conditions considered, the main equations describing thin layer flows for movement, temperature, and mix levels appear as [31–32]

$$\nabla \cdot \vec{V} = 0, \tag{1}$$

$$[(V^{\rightarrow} \cdot \nabla)\, V^{\rightarrow}] = \upsilon\, (1 + \beta^{1\,2} V^{\rightarrow} + g^{*}(\beta_T (T - T_\infty) + \beta_C (C - C_\infty)) \quad - \quad - \sigma_\rho\, (B^2 V^{\rightarrow}), \tag{2}$$

$$\vec{[(V \cdot \nabla)\, T]} = \alpha \nabla^{2} T \quad \frac{T}{C_S C_P} \quad {}^{2} + D_K \nabla\, C, \tag{3}$$

$$\left[\left(\vec{V} \cdot \nabla\right) C\right] = D \nabla^2 C + \frac{D_K}{T_m} \nabla^2 T. \tag{4}$$

Using the definition of $\vec{V}$ and $\vec{q}$, the equations (1-4) reduce to the following forms with usual notations [31-32]

$$\frac{\partial u}{\partial x} + \frac{\partial v}{\partial y} = 0, \tag{5}$$

$$\frac{\partial u \sigma B^2 u}{} + v \frac{\partial u}{} = \upsilon \left(1 + \frac{1}{}\right) \frac{\partial^2 u}{{}_2} + g^{*}\left(\beta_T (T - T_\infty) + \beta_C (C - C_\infty)\right) - \frac{u}{\partial x} \quad {}_{\partial y} \quad \beta \quad \frac{}{\partial y} \quad {}_{\rho}, \tag{6}$$

$$u\frac{\partial T}{\partial x} + v\frac{\partial T}{\partial y} = \alpha\frac{\partial^2 T}{\partial y^2} + \frac{DK}{C_S C_P}\frac{\partial C}{\partial y}\frac{\partial T}{\partial y}, \tag{7}$$

$$u\frac{\partial C}{\partial x} + v\frac{\partial C}{\partial y} = D\frac{\partial^2 C}{\partial y^2} + \frac{DK}{T_m}\frac{\partial T}{\partial y}\frac{\partial T}{\partial y}. \tag{8}$$

With

$$u = u_w(x),\ v = 0,\ T = T_w(x),\ C = C_w(x) \text{ at } y = 0, \tag{9a}$$

$$u = 0,\ T = T_\infty,\ C = C_\infty \text{ as } y \to \infty. \tag{9b}$$

Here, u and v are the velocity elements in x and y directions respectively, concentration is C, temperature is T, density is ρ, variable magnetic field is B, acceleration due to gravity is g^*, kinematic viscosity is υ, coefficient of thermal extension is β_T, solutal diffusivity of the medium is D, dynamic viscosity is μ, coefficient of solutal extensions is β_C, the specific heat capacity is C_P, thermal diffusivity is α, concentration susceptibility is C_S, thermal diffusion ratio is K_T, and mean fluid temperature is T_m.

The circumstances at the wall and the boundary level's outer edge are denoted by the subscripts w and ∞, respectively. These are the definitions of the stretching velocity, exponential temperature allocation and exponential concentration allocation:

Whereas C_0 is a parameter of the concentration allocation in the expanding surface, T_0 is a parameter of the temperature allocation, and u_0 is a velocity parameter of the stretching surface.
Now, to transform the equations (5-8) along with (9a-9b) to non-dimensional ODEs, following similarity transformation are used:

$$\eta = \sqrt{\frac{\mathrm{Re}_x}{2L}}\frac{y}{x} = \sqrt{\frac{1}{2}\mathrm{Re}_x}\frac{y}{2L}, \quad \psi = 2Lf(\eta), u = \frac{\partial \psi}{\partial y}, v = -\frac{\partial \psi}{\partial x}, \tag{13}$$

$$T(x, y) = T_\infty + (T_0 - T_\infty)e^{2L}\theta(\eta), C(x, y) = C_\infty + (C_0 - C_\infty)e^{2L}\phi(\eta).$$

On applying Eq.(13), Eq.(3) is identically satisfied whereas the remaining equations along with boundary conditions are transformed to the following non-dimensional form:

$$\left(1 + \frac{1}{\beta}\right)f''' + ff'' + 2Rie^{-3\lambda}(\theta + N\varphi) - M^2 f' - 2(f')^2 = 0, \tag{14}$$

$$\theta'' + Pr\, f\, \theta' - Pr\, f'\theta + Pr\, D_f \phi'' = 0, \tag{15}$$

$$\phi'' + Scf\phi' - Scf'\phi + ScSr\theta'' = 0. \quad (16)$$

With

$$\eta = 0: f(0) = 0, f'(0) = 1, \theta(0) = 1, \phi(0) = 1, \quad (17a)$$

$$\eta \to \infty: f'(\infty) = 0, \theta(\infty) = 0, \phi(\infty) = 0, \quad (17b)$$

Here, $\lambda =$ is the λ is location, L is the plate's characteristic length, and the primes indicate partial differentiation with regard to η, $B = B_0 e_{2L}$ is magnetic $= \frac{\beta_T(-T_\infty + T_0)L^3 g^*}{2}$ field, Gr_v is the thermal Grashof number, $Ri = Re_2$ is the mixed convection parameter, $N = \frac{(C_0 - C_\infty)^{\beta C}}{(T_0 - T_\infty)\beta T}$ is the buoyancy ratio, $Pr = \alpha v$ is the Prandtl number, $Re = uv^{0L}$ is the Reynolds number, $Sc = \frac{v}{D}$ is the Schmidt number, $D_f = \frac{DK_T (C_0 - C_\infty)}{D(-T_\infty + T)K} = \frac{0\ T}{\sigma B_0 2L}$ is the Dufour number, Sr is the Soret number and $M = \frac{}{\rho\ u_0}$ is Hartmann number.

Looking closely at Eq. (15), you see the speed patterns in mixed convection shift when dealing with thick fluids - this happens since the -direction stays tied into the math here. Though certain edge flows with such fluids sometimes allow partial simplified answers, using that method turns out messy here. So instead, researchers turned toward finding solutions for Eq. (14) that stay consistent nearby but might change farther away. Meaning, provided conditions hold, each spot lets us track how separate factors shape individual curves just there. A thin layer touching a steady-density fluid experiences heat flow, material movement, and force along its surface. To understand how much resistance slows the moving substance, computing surface friction reveals key details about that slowing effect plus how quickly warmth moves through convection. It also aids in finding values tied to convective efficiency - one related to heat exchange, another to mass transfer. These measures - relating to temperature shifts at boundaries, surface grip strength, and diffusion behavior - appear

mathematically as: $Nu_x = -\theta'(0)$, $C_f = -\frac{}{}1 + \frac{1}{}^{}f''(0)$ and $Sh_x = -\phi'(0)$.

3. Domain transformation: Semi-infinite to finite domain

Coordinate transformation $\chi = \frac{\eta}{\eta_\infty}$ and the ensuing variable modification can change the semi-infinite domain from [0, ∞)to [0,1]. Now, defining $F(\chi) = \frac{f(\eta)}{\eta_\infty}$, and $\Theta(\chi) = \frac{\theta}{\eta(\infty\eta)}$, where η_∞ is unknown finite border. On applying the aforementioned modifications, the equations (14-16) along with boundary conditions transformed to

$$\left(1+\frac{1}{\beta}\right)F'''(\chi)+\eta_\infty^2 F(\chi)F''(\chi)+2Rie^{-\frac{3\lambda}{2}}\left((\eta_\infty^3\Theta(\chi)+N\eta_\infty^3\Phi(\chi)\right)$$
$$-M^2\eta_\infty^2 F'(\chi)-2\eta_\infty^2 F'^2(\chi)=0 \quad (18)$$

$$-\frac{1}{Pr}\Theta''(\chi)+\eta_\infty^2 F(\chi)\Theta'(\chi)-\eta_\infty^2 F'(\chi)\Theta(\chi)+D_f\varphi''(\chi)=0 \quad (19)$$

$$-\frac{1}{Sc}\phi''(\chi)+\eta_\infty^2 F(\chi)\phi'(\chi)-\eta_\infty^2 F'(\chi)\phi(\chi)+Sr\Theta''(\chi)=0 \quad (20)$$

with

$$\left.\begin{aligned} &F(0)=F'(1)=0, F'(0)=1, F'(1)=0,\\ &\Theta(0)=\frac{1}{\eta_\infty},\ \Theta(1)=0, \varphi(0)=\frac{1}{\eta_\infty},\ \varphi(1)=0. \end{aligned}\right\} \quad (21)$$

4. Numerical solution using Taylor wavelet method (TWM)

Here, we tackle the nonlinear ordinary differential equations from earlier by applying the Taylor Wavelet Method numerically. Chosen for sharp accuracy and quick convergence, it handles tough boundary issues well. Through expansion in Taylor wavelet basis functions, the method turns differential equations into algebraic systems. Solutions emerge under set boundary rules, revealing patterns in speed, heat, and mix levels. Following steps laid out in sources [33–35], the process keeps outcomes stable and finely resolved.

4.1 **Velocity profile:**

Let's assume $F'''(\chi)=U^T\omega$, (22)

From Eq. (22) integrating w.r.t χ, and the range from $0\to\chi$,

$$F''(\chi)=F''(0)+U^T(B\omega+\bar{\omega}), \quad (23)$$

From Eq. (23) integrating w.r.t χ, and the range from $0\to\chi$,

$$F'(\chi)=F'(0)+\chi F''0)+U^T(B'\omega+\overline{\omega'}), \quad (24)$$

From Eq. (24) integrating w.r.t χ, and the range from $0\to\chi$,

$$F(\chi)=F(0)+\chi F'(0)+\frac{\chi^2}{2}F''0)+U^T(B''\omega+\overline{\omega''}), \quad (25)$$

Using boundary conditions (21), then the Eqs. (25) and (24) becomes,

$$F(\chi)=\chi+\frac{\chi^2}{2}F''(0)+U^T(B''\omega+\overline{\omega''}), \quad (26)$$

$$F''(0) = -1 - (B'\omega + \bar{\omega}')\Big|_{\chi=1}. \quad (27)$$

4.2 Temperature profile:

Let's assume $\Theta''(\chi) = U^T\omega$, (28)

From Eq. (28) integrating w.r.t χ, and the range from $0 \to \chi$,

$$\Theta'(\chi) = \Theta'(0) + U^T(B\omega + \bar{\omega}), \quad (29)$$

From Eq. (29) integrating w.r.t χ, and the range from $0 \to \chi$,

$\Theta(\chi) = \Theta(0) + \chi\Theta'(0) + U^T(B'\omega + \bar{\omega}')$, (30) apply boundary conditions (21), then (30) becomes,

$$\Theta(0) = \frac{-1}{\eta_\infty} - U^T\left(B'\omega + \bar{\omega}'\right)\Big|_{\chi=1}.$$

***4.3 Concentration profile*( ) :**

Let's assume $\phi''(\chi) = U^T\omega$, (31)

From Eq. (31) integrating w.r.t χ, and the range from $0 \to \chi$,

$$\phi'(\chi) = \phi'(0) + U^T(B\omega + \bar{\omega}), \quad (32)$$

From Eq. (32) integrating w.r.t χ, and the range from $0 \to \chi$,

$\phi(\chi) = \phi(0) + \chi\phi'(0) + U^T(B'\omega + \bar{\omega}')$, (33) apply boundary conditions (22) then (33) becomes,

$$\phi'(0) = \frac{-1}{\eta_\infty} - U^T(B'\omega + \bar{\omega}')\Big|_{\chi=1}. \quad (34)$$

To collocate the equations and obtain the Taylor wavelet's unknown coefficients, we can Substitute $F''''(\chi)$, $F''(\chi)$, $F'(\chi)$, $F(\chi)$, $\Theta''(\chi)$, $\Theta'(\chi)$, $\Theta(\chi)$,*and* $\phi''(\chi)$, $\phi'(\chi)$, $\phi(\chi)$. Utilize collocation steps using $\chi_i = \frac{2i-1}{2N}$, where $i = 1,2,3 \ldots N$. Pick values for that fit what the task needs.

Using the collocation points, turn things into a set of equations. The system shown here must be worked out somehow. Get it done with a method that handles such problems well. From solving the equation set, the missing parts of the Taylor wavelets come together. Using those computed values, answers to numbers (18), (19), and (20) take shape - given the conditions laid out in (17a, 17b). What comes next depends on how these pieces fit.

5. Results and discussions

A fresh look at how heat and mass move together in a magnetic field used the Taylor Wavelet Method to study Casson fluids on a rapidly expanding surface. Instead of relying solely on new data, earlier test cases without thermal or solutal mixing helped check if the method worked well. Results lined up

closely with trusted reference points, showing stability even when dealing with tangled math patterns. Strong match-ups across trials suggested this wavelet technique handles tough linked equations without losing precision.
Checking continued using a special scenario where certain values approach zero, while others change step by step. These outcomes were measured against earlier findings cited in sources [31–32]. See Table 1 - numbers match closely with what's been shared before. That fit supports how reliable and quick the Taylor Wavelet Method works when studying complex MHD flows with linked heat and substance movement.

Looking at how different settings influenced outcomes revealed patterns across the system - check out Figures 3 through 15 for visual details showing these shifts clearly.
Figures 3, 9, and 12 reveal how growth affects flow traits. From these visuals, we trace changes as the value shifts between –0.5 and 3.0 under fixed settings. Looking at the trend, higher values push up both fluid speed and the boundary layer's depth. Instead of rising steadily, heat patterns act differently - initially climbing when rises, yet differences among curves shrink across levels. Beyond a point, those same thermal readings begin to drop off slowly. Meanwhile, particle spread dips without exception across space, along with a narrower diffusion zone as climbs - clearly visible in Figure 12.

Look at Figures 4, 10, and 13 - they show how changing and affects and . With fixed at , , and using and , the graphs reveal something: speed of flow rises along with heat level when goes up (or drops), clear in Figure 4 and 10. More means more energy shifts from concentration differences into heat, cutting down resistance while boosting upward movement driven by warmth - so grows. Yet when climbs, material movement caused by heat variation gets stronger, slowing things down because motion steadies, leading to lower as shown in Figure 4. Stronger links between concentration differences and heat movement show up when values rise - pushing energy flow upward. When numbers drop instead, less material shifts because of heat changes, which helps keep energy from escaping, holding the curve higher - check Figure 10. The opposite trend appears elsewhere - look at Figure 13. As the value climbs, energy moves faster from chemical imbalance into warmth, draining the shape across the graph. Temperature-driven motion gets a boost if that number rises, building up substance amounts; yet, smaller values dull this force, flattening the plotted line.

Looking at Figures 5, 11, and 14 reveals changes in due to -location when stays constant. From these visuals, we see dipping as rises, whereas both grow. Instead, Figures 6 through 8 display effects brought by raising , then separately. With higher and , drops off - yet speed of the fluid goes up when is boosted. Because the Casson factor goes down when the fluid's yield stress goes up, raising it means less resistance inside the fluid, which thickens the flow. That extra thickness slows how fast layers move past each other, so the shift in speed drops - check Figure 6. Meanwhile, one term stands for how strong the magnet is pulling across the liquid. In fluids that carry current, a push called Lorentz fights against the way things are moving. With rising values, the force grows stronger, resisting flow and lowering the outcome - check Figure 7. Instead of just adding effects, changes in N reflect how heat and concentration-driven forces compare; when N rises, heat effects take over, boosting movement and raising the result, visible in Figure 8.
Close to the surface, values rise when increases from to then drop off further out. Since stands for how fast momentum spreads compared to mass, bigger means slower movement of into the flow - this

sharpens changes nearby. Once climbs past 1, drops across all cases, though sharper declines happen where is larger. The reason? Higher limits how far concentrations can travel away from the boundary.
Skin friction drops when the mixed convection value goes up since greater buoyancy begins to outweigh resistance caused by movement. Because upward push becomes more dominant, the drag along the surface weakens, which lowers the friction measure. As you move farther from the boundary - shown by rising similarity values - the influence of stretching and rubbing at the wall fades even more. This fading pull combines with lighter shear forces to keep pushing friction numbers downward. Together, these shifts show how lift-driven flow and shrinking grip near the sheet shape what happens across the region.
When the mixed convection value gets bigger, the thermal Nusselt number goes up - this happens because stronger buoyancy flow pushes more heat through the surface. Heat moves faster under these conditions, shown clearly by the rising Nusselt values. Moving away from the sheet, captured by a growing similarity variable, the heated layer narrows down sharply. That thinning boosts how much heat escapes close to the surface. Seen together in Figure 17, shifting forces and narrowing layers team up to sharpen heat movement.
From Figure 18, it's clear that stronger buoyancy effects slow down how fast material moves across the boundary. When the mixed convection value goes up, natural rise forces dominate, thinning out the layer where concentration changes happen close to the wall. That thinner zone means less push for molecules to move, so the transfer count called Sherwood drops. Moving farther into the fluid - higher similarity values - the surface has even less grip on what's happening, letting the exchange fade more. With distance, the whole process loses strength bit by bit. Stretching the surface pulls the liquid outward while sucking or pushing through alters its thickness and speed. A magnetic presence drags back motion like invisible resistance, changing how smoothly things flow. Thickened traits from Casson behavior also reshape movement patterns seen in Figure 19. When suction pulls fluid inward, flow lines squeeze tighter, making the friction zone thinner. Blowing pushes outward instead, stretching those same lines, which adds wobble to smooth motion. Cooling gets stronger under suction since the hot skin near surfaces shrinks in width. In contrast, when air blows out or magnets act on the system, warmth builds up, causing that heated shell to grow thicker.

6. Conclusion

This research looked into how heat and mass transfer influence magnetic convection in a Casson fluid moving across a surface that stretches rapidly, applying the Taylor Wavelet approach. Accuracy stood out clearly when outcomes matched well-known solutions under simplified conditions. Efficiency showed through consistent performance during testing phases. Results lined up closely with earlier findings where comparisons were possible. Use of the wavelet technique brought stable numerical behavior without extra complexity. Performance held steady even with varying physical parameters. Agreement improved as validation steps increased. Computational speed remained high throughout simulations. Patterns emerged smoothly from iterative calculations. Solutions adapted well to changes in boundary settings. Precision stayed strong across different test scenarios. Testing confirmed reliability under extreme values too. Outputs reflected expected trends without deviation. Consistency appeared across multiple verification checks. Model response followed logical paths each time.

Key findings include:

- Increasing the mixed convection parameter enhances velocity and temperature but reduces concentration profiles.
- Higher Dufour number and lower Soret number intensify thermal and velocity fields, while concentration decreases.
- An increase in the magnetic parameter or Casson parameter suppresses velocity due to Lorentz and viscous effects.
- The thermal and solutal buoyancy ratio strengthens flow motion, increasing velocity.
- Higher Schmidt number reduces concentration thickness due to lower mass diffusivity.
- Skin friction decreases with stronger buoyancy forces, while the Nusselt number increases and Sherwood number decreases.

A close look at the findings shows how well the Taylor Wavelet Method handles complex MHD systems where heat and mass move together in strange-thick liquids. Though tricky by nature, these flows respond clearly when this approach steps in. What stands out is its grip on twisty interactions without losing precision. Fluids that do not follow normal flow rules still reveal patterns under this technique. Even with heavy coupling, results stay steady. One thing becomes clear: messy physics can meet clean math.

Table 1. Comparison of □' 0( )values for distinct values of *Pr* with those reported by [31-32].

Pr	Keller and Magyari [32]	Srinivasacharya and Ram Reddy [31]	Present
0.5	-0.59434	-0.59438	-0.59435
1.0	-0.95478	-0.95478	-0.95475
3.0	-1.86908	-1.86908	-1.86907
5.0	-2.50014	-2.50015	-2.50014
8.0	-3.24213	-3.24218	-3.24215
10.0	-3.66038	-3.66043	-3.66043

Table 2. Computed numerical values of f□□(0), −□□(0) and −□□(0) .

Ri	*Sr*	D_f	*X*	*Pr*	f□□(0)	−□□(0)	−□□(0)

-0.5 -0.1 0.5 3.0	2.0	0.03	3.0	1.0	-1.29399 -1.28408 -1.27097 -1.22243	0.94867 0.95561 0.96278 0.98297	-0.04882 -0.03622 -0.02553 -0.00241
1.0 1.0 1.0 1.0 1.0 1.0	2.0 1.6 1.2 1.0 0.8 0.5	0.03 0.0375 0.05 0.06 0.075 0.12	0.5	1.0	-0.63185 -0.63861 -0.64526 -0.64847 -0.65151 -0.65530	1.11260 1.10891 1.10428 1.10129 1.09741 1.08763	0.07884 0.15155 0.22421 0.26055 0.29693 0.35177
1.0 1.0	0.2 0.1	0.3 0.6			-0.65421 -0.64526	1.05427 1.00119	0.40841 0.43038
1.0 1.0 1.0 1.0	2.0	0.03	0.1 0.5 1.0 3.0	1.0	-0.18799 -0.63185 -0.94660 -1.26070	1.17618 1.11260 1.05527 0.96766	0.10589 0.07884 0.04971 -0.01910
1.0 1.0 1.0 1.0	2.0	0.03	0.5	0.5 1.0 3.0 5.0	-0.58379 -0.63185 -0.70730 -0.73931	0.75881 1.11260 2.03606 2.70661	0.23051 0.07884 -0.13554 -0.60416

Table 3. Values of skin friction and Nusselt number for different values of M when $S = 2.0, \square = 1, M = 1, N = 1, D = 0.03, \square = 0.5, Ri = 1.0, \Pr = 1.0.$ $r \quad f$

M	$\square \quad 1 \square$ $-\square 1 + \_\square f \square\square(0)$ $\square \square\square$	$-\square\square(0)$	$-\square\square(0)$
0.1	26.8888	5.957	5.957
0.2	35.3868	5.95971	5.95971
0.3	35.3868	5.95971	5.95971
0.4	49.6856	5.96407	5.96407

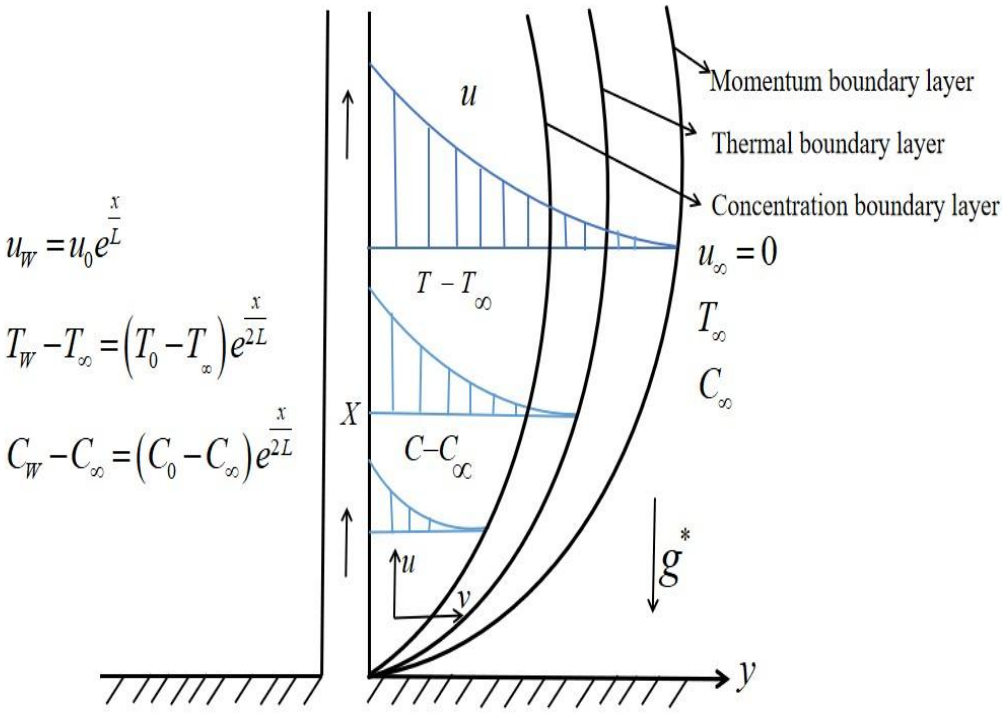

Fig. 1: Physical model and Coordinate system.

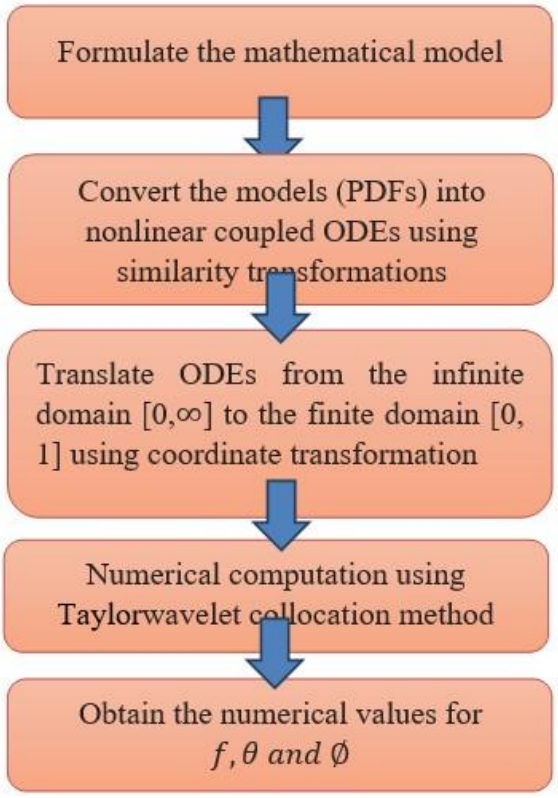

Fig. 2: Flow chart

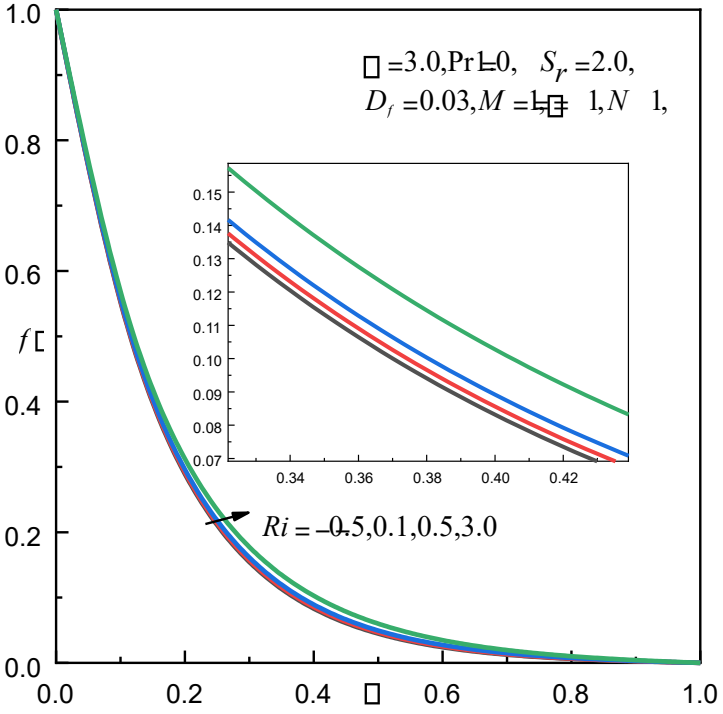

Fig. 3: Impact of Ri on $f'(\eta)$.

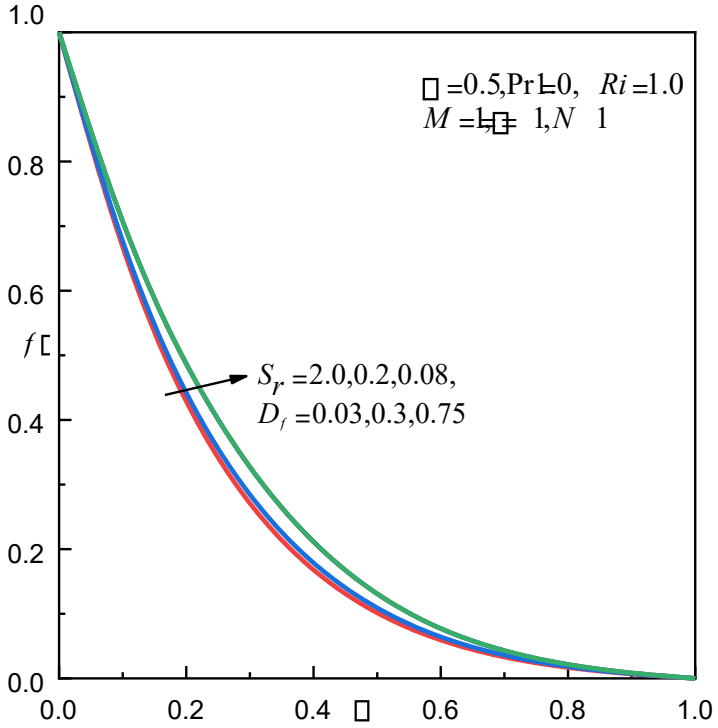

Fig. 4: Impacts of $Sr and D_f$ on $f'(\eta)$.

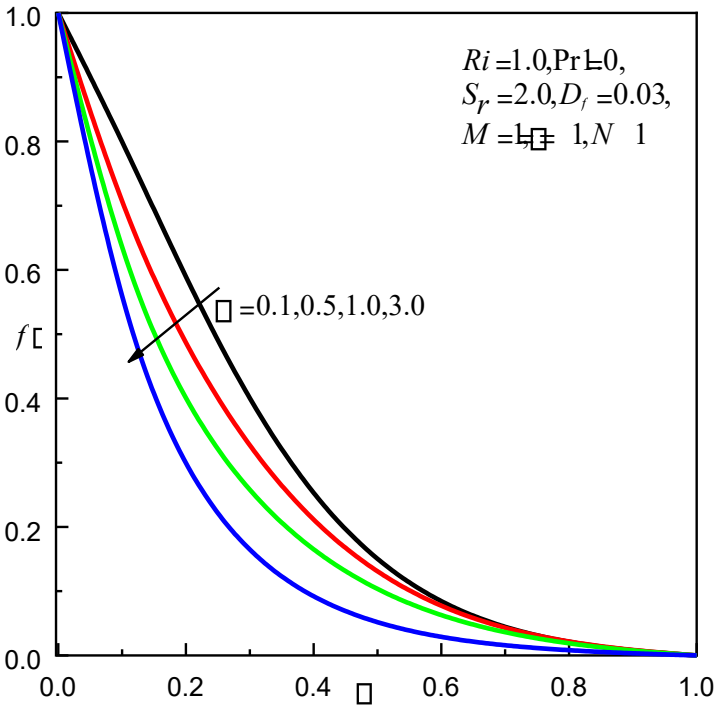

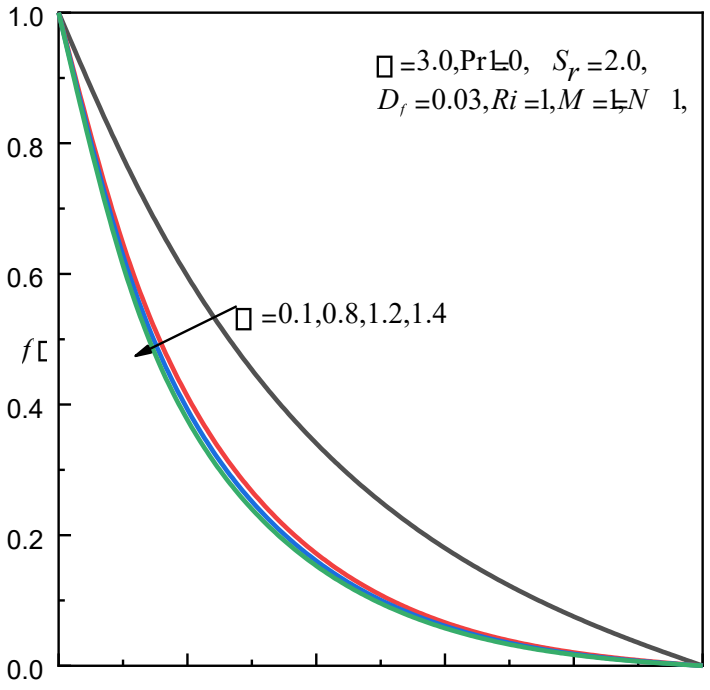

Fig. 5: Impact of on f ( ) .

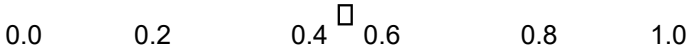

Fig. 6: Impact of on f ( ) .

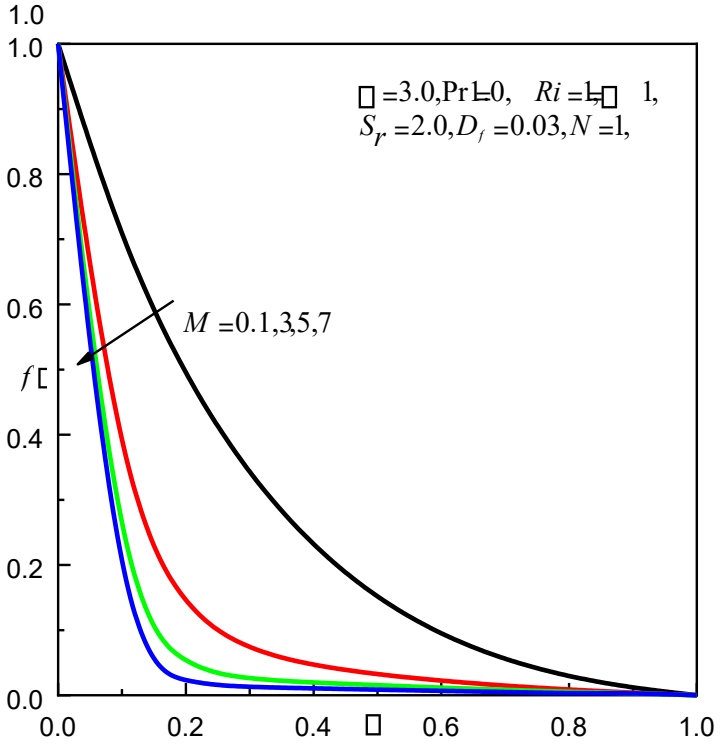

Fig. 7: Impact of M on $f'(\eta)$.

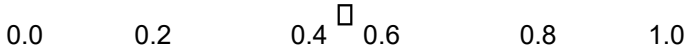

Fig. 8: Impact of N on $f'(\eta)$.

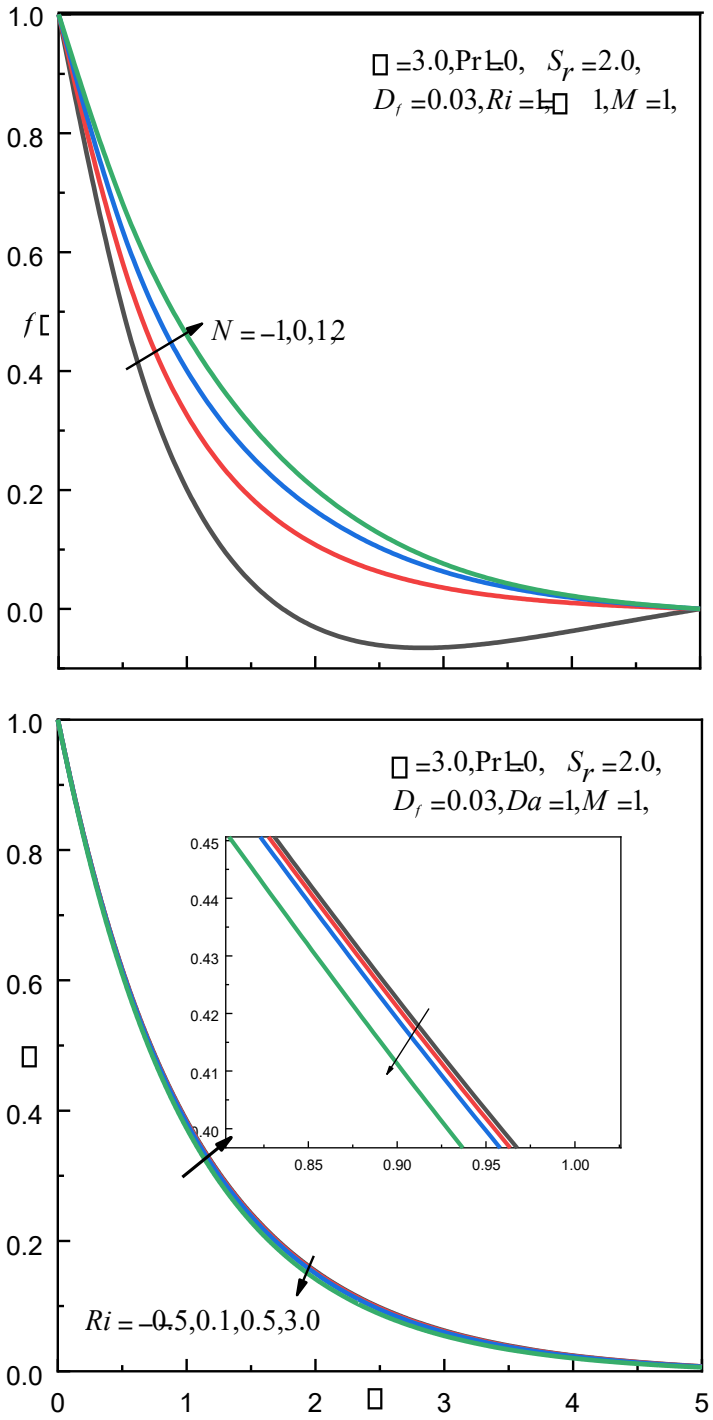

Fig. 9: Impact of Ri on ( ).

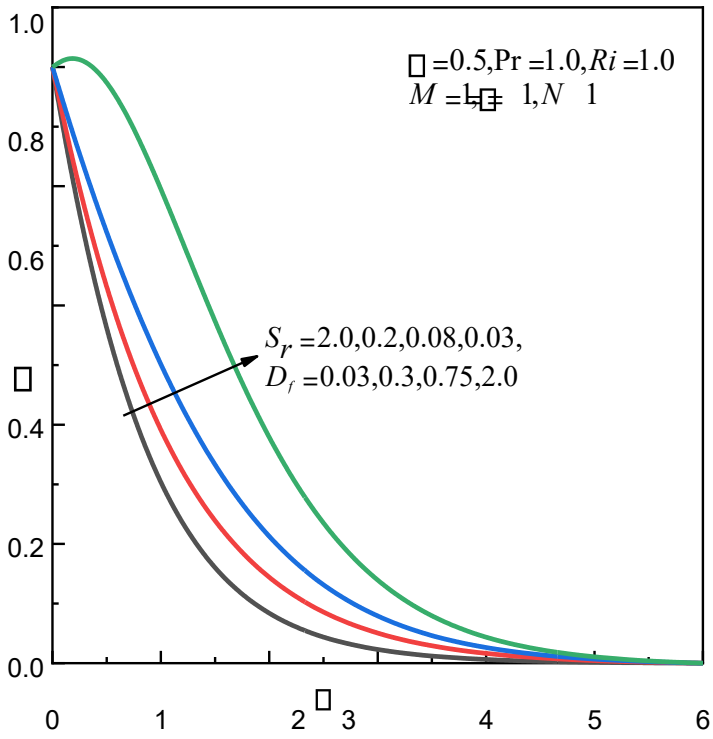

Fig. 10: Impact of Sr and D_f on ( ).

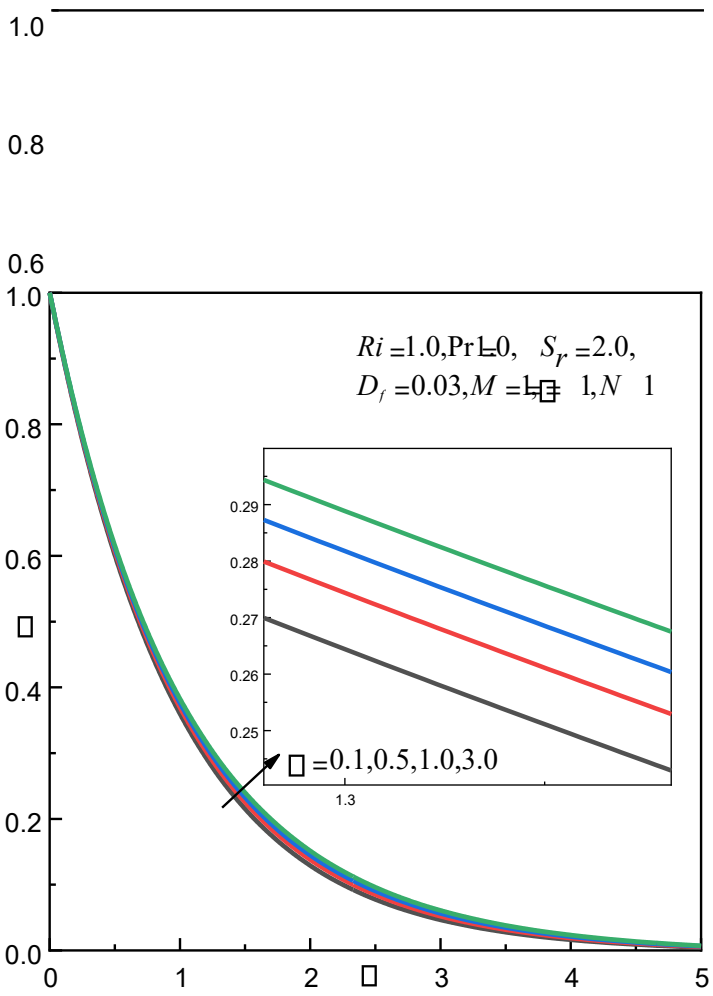

Fig. 11: Impact of on ( ).

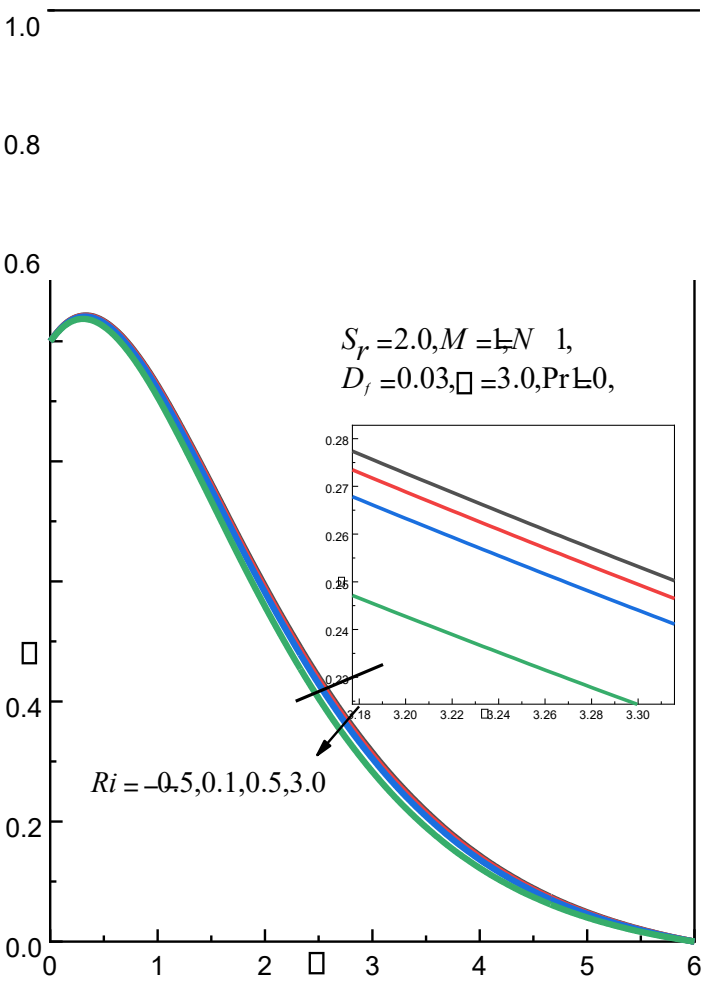

Fig. 12: Impact of Ri on $\theta(\eta)$.

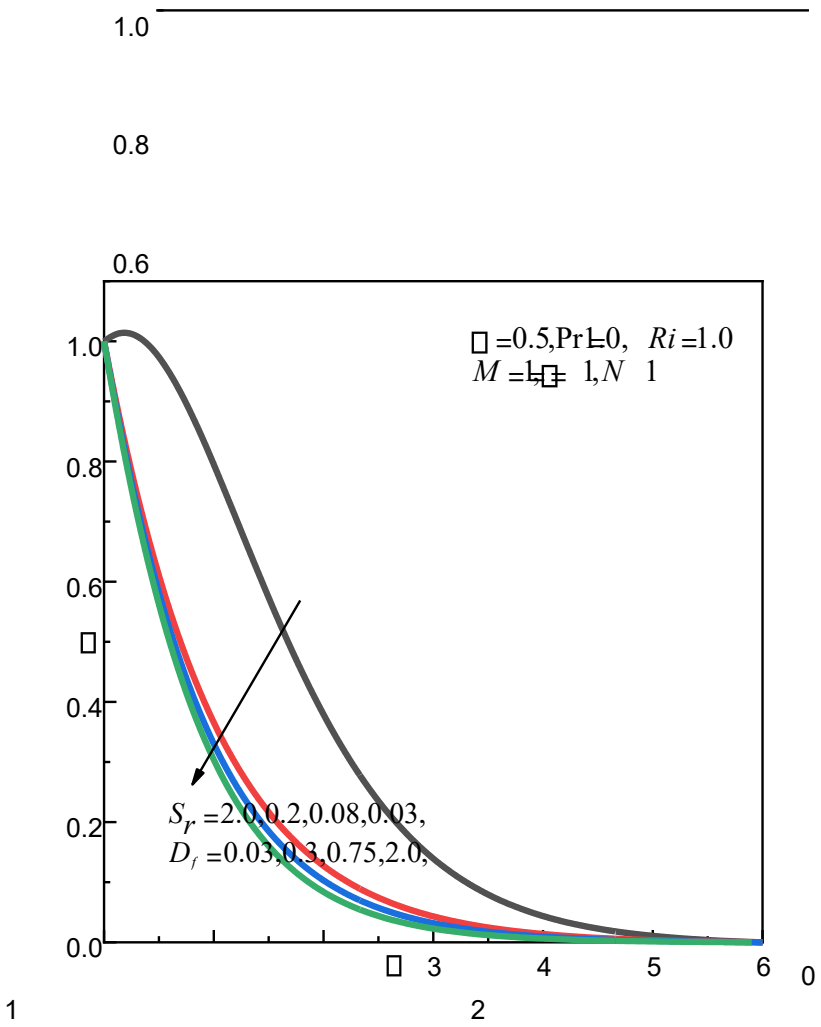

Fig. 13: Impact of $Srand D_f$ ( ) .

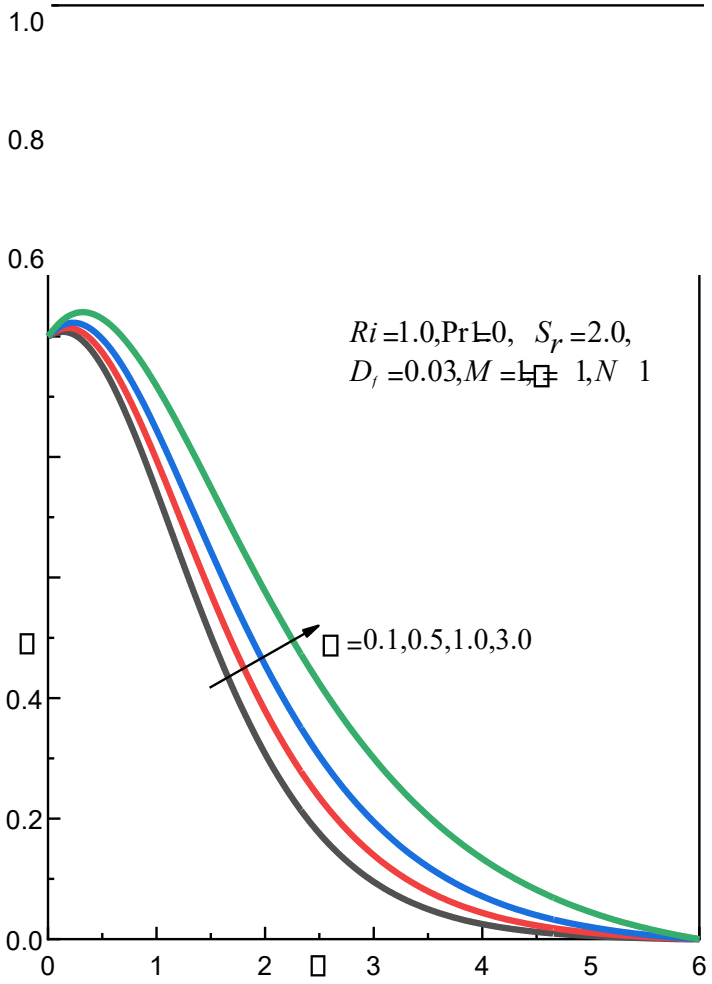

Fig. 14: Impact of on ( ) .

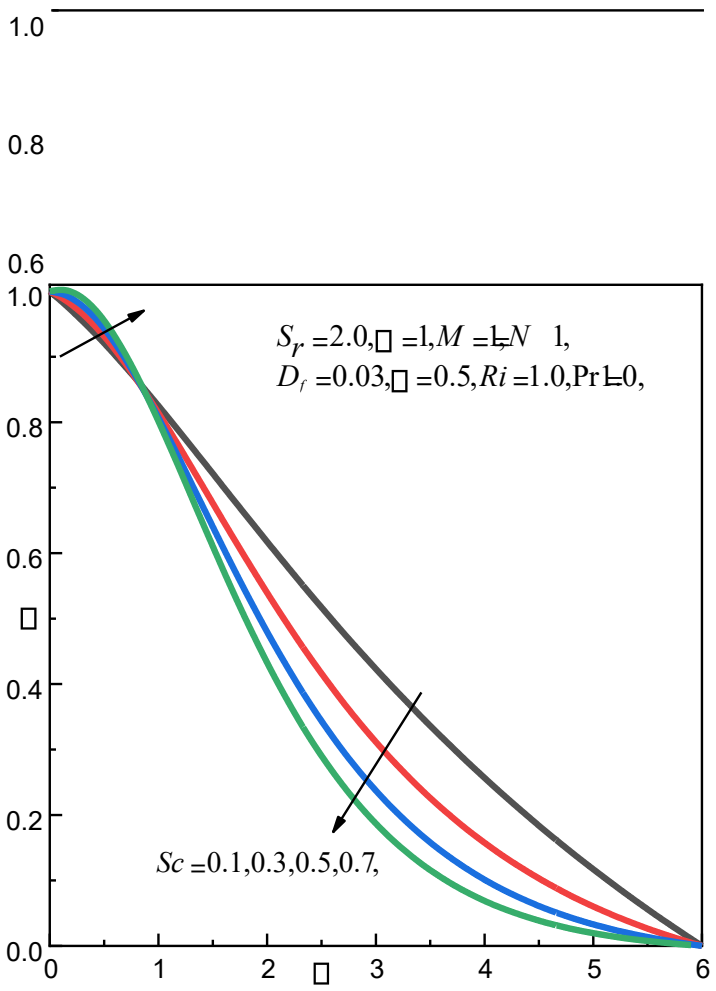

Fig. 15: Impact of Sc on ( ) .

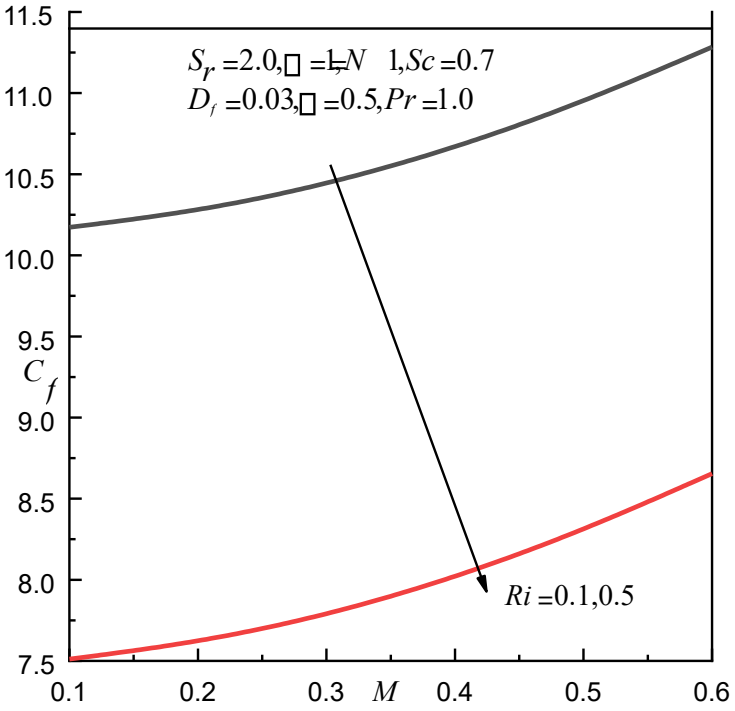

Fig. 16: Impact of Ri on C_f.

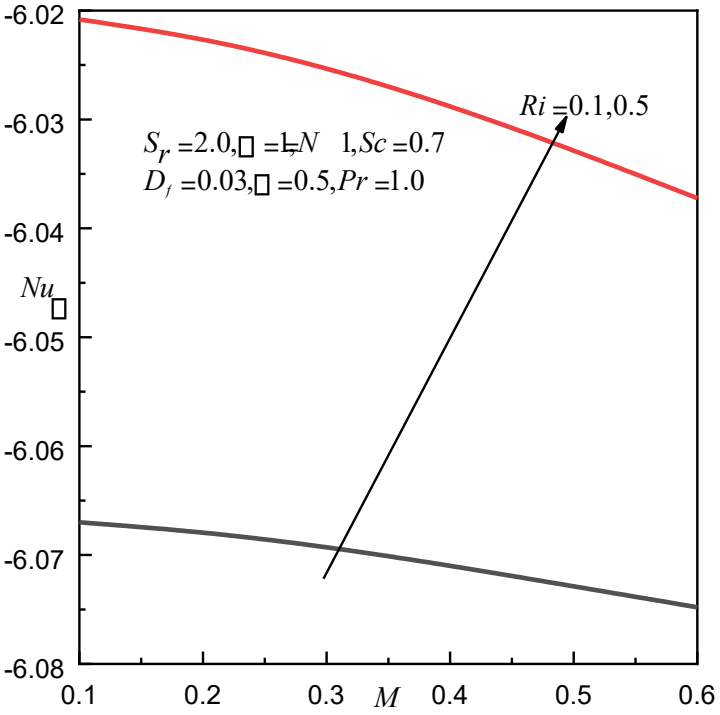

Fig. 17: Impact of Ri on Nu□.

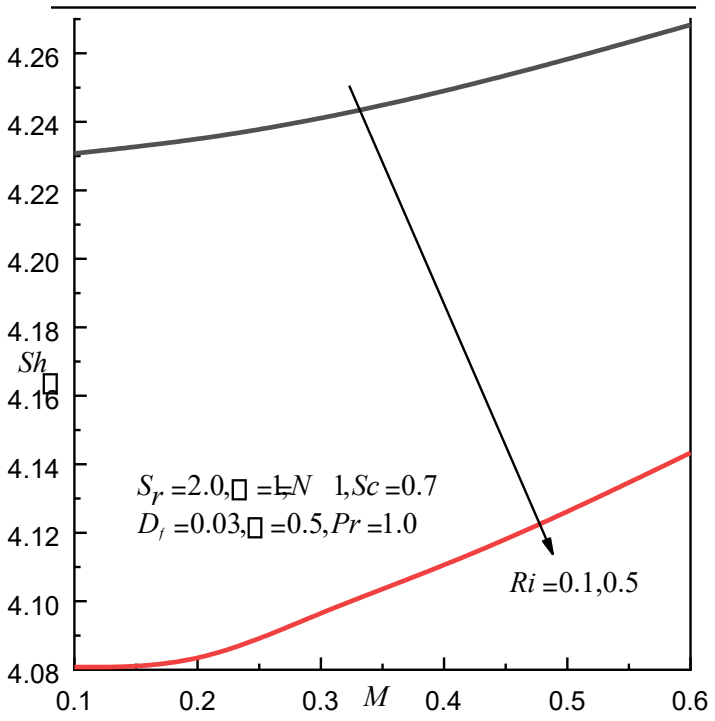

Fig. 18: Impact of Ri on Sh .

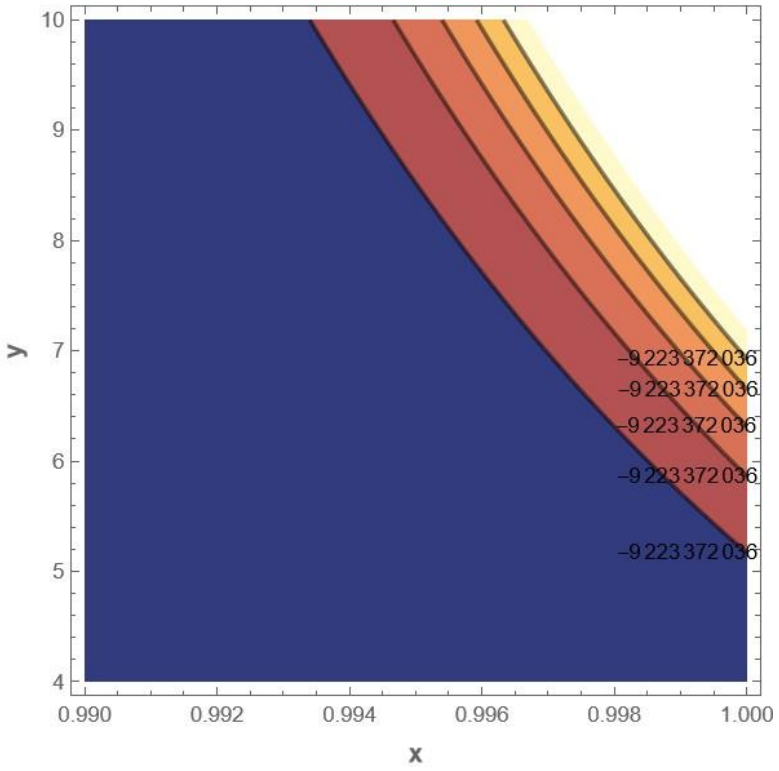

Fig. 19: Stream line.

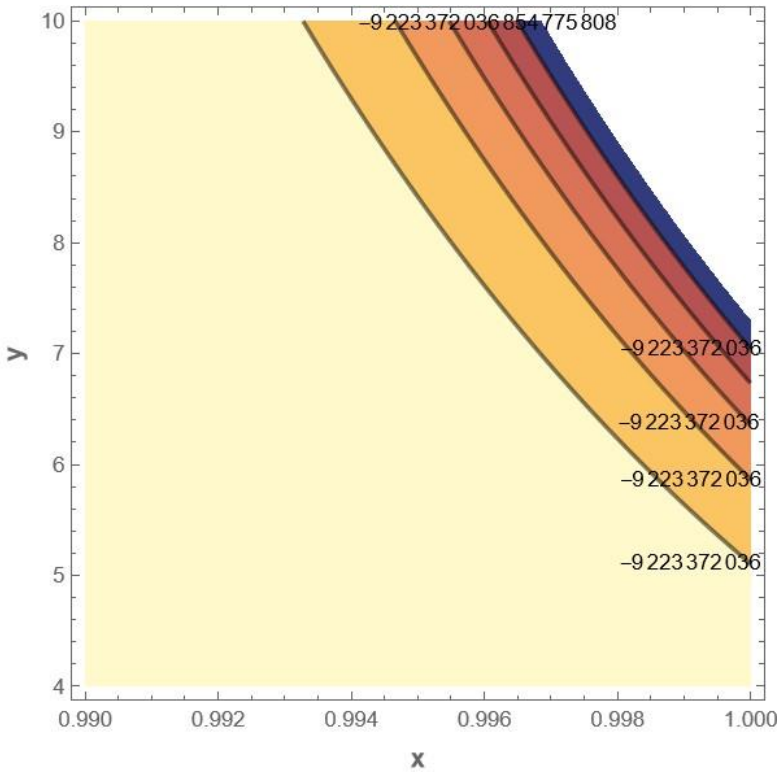

Fig. 20: Isothermal line.